# Deterministic and Robust Volt-var Control Methods of Power System Based on Convex Deep Learning

Qing Ma, *Member*, *IEEE*, and Changhong Deng, *Member*, *IEEE*

***Abstract*—Volt-var control (VVC) is essentially a non-convex optimization problem due to the non-convexity of power flow (PF) constraints, resulting in the difficulty in obtaining the optimum without convexity conversion. The existing second-order cone method for the convexity conversion often leads to a sharp increase in PF constraints and optimization variables, which in turn increases the optimization difficulty or even leads to optimization failure. This paper first proposes a deterministic VVC method based on convex deep learning power flow (DLPF). This method uses the input convex neural network (ICNN) to establish a single convex mapping between state parameters and node voltage to complete the convexity conversion while the optimization variables only correspond to reactive power equipment, which can ensure the global optimum with extremely fast computation speed. To cope with the impact brought by the uncertainty of distributed energy and omit the additional worst scenario search of traditional robust VVC, this paper proposes robust VVC method based on convex deep learning interval power flow (DLIPF), which continues to adopt ICNN to establish another convex mapping between state parameters and node voltage interval. Combining DLIPF with DLPF, this method decreases the modeling and optimization difficulty of robust VVC significantly. Test results on 30-bus, 118-bus, and 200-bus systems prove the correctness and rapidity of the proposed methods.**

***Index Terms*—Volt-var control, convexity conversion, convex deep learning, power flow.**

## I. Introduction

THE problem of voltage and reactive power in local grid varying wildly and randomly brought by the uncertainty of distributed energy spawns the upgrade of volt-var control (VVC) to be more accurate and faster [1] - [3]. Due to the nonlinear and nonconvex nature of power flow (PF) constraints in the optimization model, VVC is essentially a kind of non-convex and nonlinear programming problem, which can easily fall into local optimum with no pretreatment [4], [5]. For the optimal control strategy to coordinate various types of reactive power devices, existing studies generally adopt second-order cone (SOC) to transform PF constraints from non-convex to convex in advance [6]-[9]. However, the use of SOC will cause a sharp increase in optimization variables and PF constraints, which, in turn, greatly increases the optimization complexity and computation time [10], and even leads to failure, which is contrary to the requirement of upgrading the computation accuracy and speed of VVC. Therefore, it is important to find a transformation method that can both complete the convexity conversion and significantly reduce the numbers of variables and constraints.

Because of the time-consuming nature of traditional PF methods (such as Newton-Raphson method) serving as basic tools for VVC, voltage stability analysis, etc., deep learning (DL) method has been introduced into PF in recent years [11] - [13]. The well-trained deep learning power flow (DLPF) model can realize the end-to-end and high-precision mapping between the state parameters and PF results (such as node voltage and phase angle), eliminating the PF constraints and iterative process required by the traditional methods. However, the nonlinear mapping realized by the conventional DLPF is still non-convex. Therefore, to accelerate the computation speed and ensure the global optimum when DLPF is applied to VVC, it is also necessary to perform the convexity conversion for DLPF.

As the vigorous development and uncertainty of distributed energy, traditional VVC should upgrade to deal with the problem that deterministic VVC (DVVC) strategy may not adapt to the actual scenarios. Recently, the methods for dealing with uncertainty mainly include stochastic programming and robust optimization. Stochastic programming generally converts uncertain programming into deterministic one by the simulation of random variables to achieve probabilistic optimum [14] - [17]. However, stochastic programming requires deterministic characterization of random variables by establishing probability density functions. But it is often difficult to obtain the true distributions of random variables, and the artificially set distributions always bring large error, resulting in a large difference between the derived control strategy and the actual demand.

Robust optimization does not require the establishment of deterministic distributions, but only the range of random variables. At present, robust VVC (RVVC) is mainly divided into three categories. The first [18]-[20] is to directly use lin-

Manuscript received: February 2, 2023; revised: June 5, 2023; accepted: August 11, 2023. Date of CrossCheck: August 11, 2023. Date of online publication: October 13, 2023.



Q. Ma (corresponding author) and C. Deng are with the school of Electrical Engineering and Automation, Wuhan University, Wuhan, China (e-mail: 747942466@qq.com; dengch@whu.edu.cn).

DOI: 10.35833/MPCE.2023.000057

ear PF to convert the uncertainty constraints of distributed energy into the original VVC constraints, but linear PF always brings large errors.

The second [21]-[24] is to establish a two-stage robust optimization model, which optimizes the master problem and sub-problems separately in each iteration for narrowing the gap between the upper and lower bounds of objective function until convergence. This type of RVVC still has two drawbacks. ① The establishment of mathematical model is too complex, which needs lots of mathematical techniques such as SOC, dual transformation, big-*M* method to transform the original problem. ② The master problem has to add new variables and constraints formed by the subproblem in each iteration, and the subproblem is difficult to solve as its optimization in each iteration should take the uncertainty of random variables into account, resulting in a significant increase in the solution time compared with DVVC. Reference [21] shows that the solution time of two-stage RVVC reaches about 25 times of DVVC when the forecasting error of distributed energy reaches 30%.

The third [25] - [27] is the worst scenario method based RVVC (WSM-RVVC), whose core idea is to find and achieve the optimal operation of the worst scenario. The main idea of WSM-RVVC is clear and the modeling is simple. However, in each iteration, the worst scenario search needs to be conducted in advance, which also takes a long time.

Based on the summary of existing DVVC and RVVC, this paper proposes a new RVVC method based on convex DL whose main contributions are described as follows.

1) A DVVC method based on convex DLPF is proposed. This method applies the convex DLPF to VVC, which builds the convex mapping between the state parameters and node voltage by adopting the input convex neural network (ICNN), and eliminates the non-convex and numerous PF constraints of traditional methods. As it makes the objective function and constraints of VVC fully convex with respect to the optimization variables, the solution complexity can be greatly reduced on the basis of ensuring the global optimum of control strategy.

2) An RVVC method based on convex deep learning interval power flow (DLIPF) is proposed. On the basis of using DLPF for convexity conversion of PF constraints, this method continues to use ICNN to build another convex mapping between state parameters and node voltage interval, which directly converts the uncertainty of distributed energy through the unequal voltage constraints, and avoids the complex model transformation of two-stage RVVC and the worst scenario search of WSM-RVVC. It makes the modeling of RVVC simple and clear, and makes the optimization convenient and fast.

The remainder of this paper is organized as follows. Section II is the mathematical model of VVC. Section III proposes convex DLPF based DVVC method. Convex DLIPF based RVVC method is elaborated in Section IV. The numerical test results are demonstrated in Section V. Section VI presents the conclusion.

## II. Mathematical Model of VVC

### A. Basic Mathematical Model

To improve the voltage quality of power system, VVC usually selects voltage deviation as the optimization object. The mathematical model is commonly constructed as:

$$\begin{cases} \min F = \sum_{i=1}^{n} \|V_i - V_{i,tar}\|_2^2 \\ \text{s.t. } P_{Gi} - P_{Li} - V_i \sum_{j=1}^{n} V_j (G_{ij}\cos\delta_{ij} + B_{ij}\sin\delta_{ij}) = 0 \\ \quad Q_{Gi} + Q_{Ci} - Q_{Li} - V_i \sum_{j=1}^{n} V_j (G_{ij}\sin\delta_{ij} - B_{ij}\cos\delta_{ij}) = 0 \\ \quad V_{i\min} \le V_i \le V_{i\max} \\ \quad CQ_{i\min} \le CQ_i \le CQ_{i\max} \end{cases} \tag{1}$$

where $F$ is the objective function; $n$ is the number of system nodes; $V_i$ and $V_{i,tar}$ are the voltage and target value of node $i$, respectively; $V_{i\min}$ and $V_{i\max}$ are the lower and upper limites of $V_i$, respectively; $P_{Gi}$ and $Q_{Gi}$ are the active and reactive power outputs of generators connected to node $i$, respectively; $Q_{Ci}$ is the reactive power compensation of node $i$; $P_{Li}$ and $Q_{Li}$ are the active and reactive loads of node $i$, respectively; $G_{ij}$ and $B_{ij}$ are the conductance and susceptance of the line connecting nodes $i$ and $j$, respectively; $\delta_{ij}$ is the phase angle difference between nodes $i$ and $j$; and $CQ_{i\max}$ and $CQ_{i\min}$ are the upper and lower regulation limits of the reactive power equipment connected to node $i$ $CQ_i$, respectively. The first two constraints are active and reactive power balance constraints of nodes, respectively, the third is state variable constraint (node voltage constraint), and the fourth is control variable constraint (reactive equipment regulation constraint).

In (1), as $V$, $\delta$, and $Q_C$ are all needed to be counted, and the first two constraints need to be established for each node, the PF equations are not only non-convex and nonlinear, but also characterized by a massive number, whose calculation formula is shown in (2), which is nearly twice the number of nodes, resulting in VVC to be essentially a non-convex and nonlinear optimization problem that is extremely complex. Direct solution without convexity conversion is prone to problems such as falling into local optimum and slow computation speed. When the system size is large, the obtained control strategy may even fail. Thus, it is important to conduct the convexity conversion of PF constraints.

$$C_{PF} = 2(n-1) - n_{PV} \tag{2}$$

where $C_{PF}$ is the number of PF constraints; and $n_{PV}$ is the number of permanent voltage (PV) nodes.

### B. Convexity Conversion of PF Constraints Based on SOC

According to [9], the PF constraints transformed by SOC can be expressed as:

$$\sum_{e:j\to e} P_{je} + P_{Lj} = P_{Gj} + \sum_{i:i\to j} (P_{ij} - h_{ij} r_{ij}) \tag{3}$$

$$\sum_{e:j\to e} Q_{je} + Q_{Lj} = Q_{Gj} + \sum_{i:i\to j} (Q_{ij} - h_{ij} x_{ij}) \tag{4}$$

$$v_j = v_i - 2(r_{ij}P_{ij} + x_{ij}Q_{ij}) + (r_{ij}^2 + x_{ij}^2)h_{ij} \tag{5}$$

$$\left\| \begin{matrix} 2P_{ij} \\ 2Q_{ij} \\ h_{ij}-v_i \end{matrix} \right\|_2 \le h_{ij}+v_i \tag{6}$$

$$(\delta_i-\delta_j)-(x_{ij}P_{ij}-r_{ij}Q_{ij})/(V_i^cV_j^c)=0 \tag{7}$$

where $P_{ij}$ and $Q_{ij}$ are the active and reactive power flowing from node $i$ to node $j$ on line $i$-$j$, respectively; $v_i$ is the mode square of the voltage of node $i$; $h_{ij}$ is the mode square of the current of line $i$-$j$; $\delta_i$ and $\delta_j$ are the phase angles of nodes $i$ and $j$, respectively; $r_{ij}$ and $x_{ij}$ are the resistance and reactance of line $i$-$j$, respectively; and $V_i^c$ and $V_j^c$ are the constants usually taken as 1.

Although the PF constraints can be converted into convex through SOC, it will cause a sharp increase in the number of PF constraints and optimization variables. In terms of PF constraints, (3) and (4) are nodal active and reactive power balance constraints, which correspond to the original PF constraints. Formulas (5)-(7) are line constraints of voltage balance, power balance, and phase angle balance, respectively, which should be valid for all lines. Therefore, the number of PF constraints increases after the convexity conversion is 3 times that of lines. Due to the connection between different nodes, the number of lines is often much larger than that of nodes, so the number of PF constraints obtained by SOC transformation will be much larger than that of original PF constraints. In terms of optimization variables, the active power, reactive power, and current of lines are added, so the number of added variables is also 3 times that of lines. In summary, although SOC can transform VVC into a convex problem that can theoretically converge to global optimum, the proliferation of the dimension of optimization variable sharply expands the feasible space, which, in combination with the proliferation of PF constraints, significantly increases the difficulty in finding the optimum. These drawbacks will be more prominent when the system size is large.

To validate the computation burden increased by SOC convexity conversion, Table I presents the number of PF constraints, the number of optimization variables, and the average calculation time using SOC-based VVC for IEEE 30-bus system, IEEE 118-bus system, and Illinois 200-bus system of USA. In Table I, the values before and after the arrow "→" indicate numbers of PF constraints or optimization variables before and after the SOC convexity conversion, respectively.

TABLE I
CALCULATION TIME COMPARISON FOR SOC-BASED VVC IN DIFFERENT SYSTEMS

| Test system | Number of PF constraints | Number of optimization variables | Average calculation time (s) |
|---|---|---|---|
| 30-bus | 53→176 | 58→181 | 5.35 |
| 118-bus | 181→739 | 234→792 | 256.41 |
| 200-bus | 350→1085 | 398→1133 | 380.31 |

As shown in Table I, with the increasement of system scale, the impact of using SOC for convexity conversion on VVC becomes increasingly obvious. Both the number of PF constraints and the number of optimization variables show a sharp increase compared with those of the original problem, ultimately leading to a significant decrease in the VVC optimization speed. Hundreds of seconds of optimization is obviously not suitable for online VVC, especially for the system with distributed energy access.

## III. CONVEX DLPF BASED DVVC METHOD

### A. Convex DL Model Based on ICNN

To address the shortcomings of convexity conversion of SOC applied to VVC, this paper adopts ICNN proposed in [28], [29] to complete the convexity conversion of PF constraints and interval PF described in the following text. As shown in (8) and Fig. 1, the differences between ICNN and conventional DL are as follows: ① ICNN sets the weight parameters of hidden layers to be non-negative and the activation function to be a non-decreasing convex function; ② to compensate for the possible degradation of model fitting ability caused by setting all the weight parameters of hidden layers non-negative, ICNN adds a direct connection of the input layer with each hidden layer by referring to residual network [30].

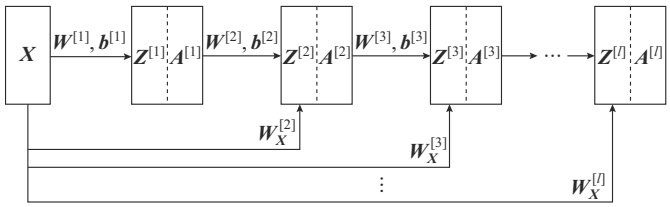


Fig. 1. DL model architecture of ICNN.

$$\begin{cases} \boldsymbol{Z}^{[l]}=\boldsymbol{W}^{[l]}\boldsymbol{A}^{[l-1]}+\boldsymbol{W}_X^{[l]}\boldsymbol{X}+\boldsymbol{b}^{[l]} \\ \boldsymbol{A}^{[l]}=\boldsymbol{g}^{[l]}(\boldsymbol{Z}^{[l]}) \\ \boldsymbol{W}^{[l]}\ge \boldsymbol{0} \\ \boldsymbol{g}^{[l]}\sim convex \end{cases} \tag{8}$$

where $\boldsymbol{Z}^{[l]}$ is the linear output of layer $l$; $\boldsymbol{A}^{[l]}$ and $\boldsymbol{A}^{[l-1]}$ are the nonlinear outputs of layer $l$ and layer $l-1$, respectively; $\boldsymbol{X}$ is the state parameter of power system; $\boldsymbol{W}^{[l]}$ and $\boldsymbol{b}^{[l]}$ are the weight and bias parameters of layer $l$, respectively; $\boldsymbol{W}_X^{[l]}$ is the weight parameter corresponding to the direct connection; and $\boldsymbol{g}^{[l]}$ is the activation function.

The backpropagation of ICNN is given in (9), which is similar to conventional DL, except for the addition of the derivation for $\boldsymbol{W}_X^{[l]}$.

$$\begin{cases} \mathrm{d}\boldsymbol{Z}^{[l]}=\mathrm{d}\boldsymbol{A}^{[l]}*\boldsymbol{g}'^{[l]}(\boldsymbol{Z}^{[l]}) \\ \mathrm{d}\boldsymbol{W}^{[l]}=\mathrm{d}\boldsymbol{Z}^{[l]}(\boldsymbol{A}^{[l-1]})^{\mathrm{T}} \\ \mathrm{d}\boldsymbol{W}_X^{[l]}=\mathrm{d}\boldsymbol{Z}^{[l]}\boldsymbol{X}^{\mathrm{T}} \\ \mathrm{d}\boldsymbol{b}^{[l]}=\mathrm{d}\boldsymbol{Z}^{[l]} \\ \mathrm{d}\boldsymbol{A}^{[l-1]}=(\boldsymbol{W}^{[l]})^{\mathrm{T}}\mathrm{d}\boldsymbol{Z}^{[l]} \end{cases} \tag{9}$$

where * represents the multiplication of the elements at the same position in two matrices of the same size; and $\boldsymbol{g}'$ is the derivative of $\boldsymbol{g}$.

It is easy to prove the convexity of ICNN: ① in the linear

calculation part of (8), since $\boldsymbol{W}^{[l]}$ is non-negative parameter, it is obvious that $\boldsymbol{Z}^{[l]}$ is convex with respect to $\boldsymbol{A}^{[l-1]}$; ② in the nonlinear calculation part of (8), as $\boldsymbol{g}^{[l]}$ is a non-decreasing and convex function, $\boldsymbol{A}^{[l]}$ is convex with respect to $\boldsymbol{Z}^{[l]}$; ③ according to [31], the composition of a convex function and a convex non-decreasing function is also convex. As the output of each DL layer is the input of the next layer, ICNN is essentially a nested composition of multi-layer convex functions, so the final output of the ICNN is convex with respect to the input.

To test the convexity conversion ability of ICNN, Griewank function is adopted to test the effectiveness and efficiency of optimization methods. The expression of Griewank function is given as:

$$G(x_1,x_2,...,x_n)=1+\frac{1}{4000}\sum_{i=1}^{n}x_i^2-\prod_{i=1}^{n}\cos\frac{x_i}{\sqrt{i}} \tag{10}$$

where $x_1$, $x_2$, ..., $x_n$ are the $n$-dimensional input variables.

To make use of contour lines to visually reflect the non-convexity of Griewank function and avoid the influence of other variables on the value of Griewank function, this paper sets two-dimensional input variables for analysis. Figure 2 shows the contour lines formed by true values of Griewank function for $x_1, x_2 \in [-500, 500]$ at function values equal to 20, 40, 60, 80, 100, respectively. Figure 3 shows the contour lines formed by ICNN fitted values of Griewank function with the same ranges of $x_1$, $x_2$, and function values. The small graphs at the center of Figs. 2 and 3 are the enlarged contour plots drawn by the two above methods. Figure 4 shows the synthetic contour map of the two methods.

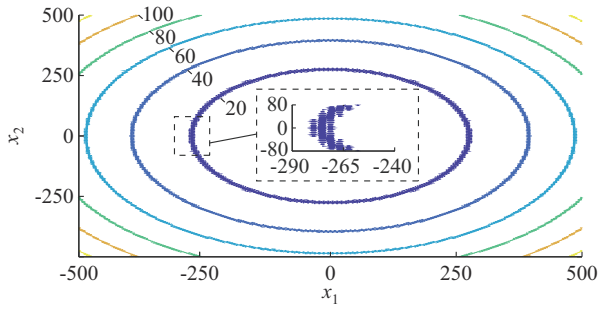


Fig. 2. Contour lines formed by true values of Griewank function.

As observed in Fig. 2, due to the non-convexity of Griewank function, the contours at different values all show a non-convex form of non-smooth, dense, and uneven distribution, indicating that the function has many local optimal points around any set value. As observed in Fig. 3, after the convexity conversion by ICNN, the contours made at any value are totally smooth and convex. The synthetic contour map in Fig. 4 shows that the contour lines formed by ICNN are completely in the envelope formed by the contour lines of true values, indicating that the error of fitting Griewank function by ICNN is extremely small. The above results demonstrate that ICNN can successfully complete convexity conversion with a high fitting accuracy.

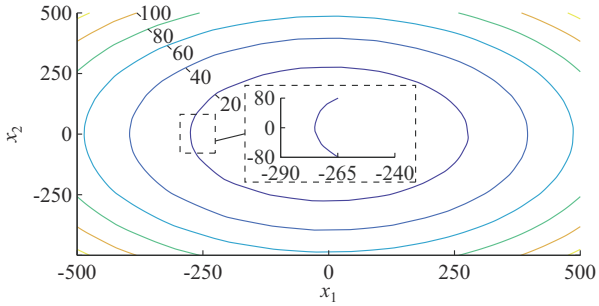


Fig. 3. Contour lines formed by ICNN fitted values of Griewank function.

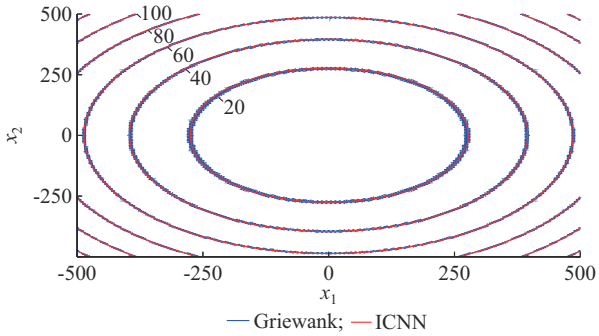


Fig. 4. Synthetic contour map of two methods.

### B. DVVC Using Convex DLPF

When applying ICNN to the convexity conversion of DVVC, the required operation is simply replacing the original PF constraints by the convex mapping between state parameters (including $P_L$, $Q_L$, $P_G$, $CQ$) and the node voltage formed by ICNN. Unlike SOC that requires a certain sacrifice of computation accuracy and a significant increase in the numbers of PF constraints and optimization variables to complete the convexity conversion, ICNN can fulfill the convex relationship of the node voltage with respect to state parameters with high accuracy, at the expense of little error between the model prediction voltage and the label value, thus greatly reducing the optimization complexity of DVVC. The mathematical model with convex DLPF based on ICNN can be expressed as:

$$\begin{cases} \min \sum_{i=1}^{n}\|V_i - V_{i,tar}\|_2^2 \\ \text{s.t. } V = ICNN_{PF}(P_G, P_L, Q_L, CQ) \\ \quad V_{i\min} \le V_i \le V_{i\max} \\ \quad CQ_{i\min} \le CQ_i \le CQ_{i\max} \end{cases} \tag{11}$$

where $ICNN_{PF}$ is the well-trained ICNN of convex DLPF.

Based on the use of ICNN, in order to match the convex DLPF model with physical information of power system while maintaining stronger generalizability, the scheme in [11] is adopted by adding the deviation loss functions of active and reactive power calculated by the predicted voltage and the physical information, like $r_{ij}$ and $x_{ij}$ of lines, to the training loss function. The stop condition of ICNN training is that the average voltage prediction error for 1000 test samples is less than 0.0002 p.u..

$$\begin{cases} \nabla_{\omega} J(\omega) = \dfrac{\partial (J(V)+J(P)+J(Q))}{\partial V} \dfrac{\partial V}{\partial \omega} \\ J(V) = \| V_f(S|\omega) - V_*(S) \|_2^2 \\ J(P) = \| P_f(V) - P_* \|_2^2 \\ J(Q) = \| Q_f(V) - Q_* \|_2^2 \end{cases} \tag{12}$$

where $\omega$ is the $ICNN_{PF}$ parameter; $J(\omega)$ is the loss function for training $\omega$; $J(V)$, $J(P)$, and $J(Q)$ are the loss functions of node voltage, active power, and reactive power, respectively; $\partial$ is the bias derivative operation; $V_f$, $P_f$, and $Q_f$ are the predicted values of node voltage, active power, and reactive power, respectively; and $V_*$, $P_*$, and $Q_*$ are the corresponding label values.

## IV. Convex DLIPF Based RVVC Method

Since it is clear and simple to implement the WSM-RVVC, which has a higher accuracy compared with the linear PF based RVVC and a simpler modeling process compared with the two-stage RVVC, this paper only elaborates on WSM-RVVC and improves it to form the convex DLIPF based RVVC method.

### A. WSM-RVVC

The essence of WSM-RVVC is finding the set of random variables that can make node voltage the worst corresponding to the current system state and optimal control strategy first, and then complete the upgrade of optimal control strategy in the corresponding extreme scenario. The iteration continues until the optimal control strategy makes the voltage range of each node meet the operation constraints. Therefore, the key to completing WSM-RVVC lies in: ① how to find two sets of random variables corresponding to the maximum and minimum extreme node voltage in the uncertain range; ② how to find the optimal control strategy in the feasible space of control variables, which can meet all constraints and make the objective function reach the minimum in the two extreme scenarios.

For the above two key problems, the common practice in the existing literature is to establish a two-level optimization model. The lower model mainly uses the worst scenario method (WSM) to determine the set of random variables corresponding to the two extreme scenarios, i.e., when the maximum and minumim extreme node voltages occur, respectively. It takes the node voltage as the target function, the random variables as the control variables, and the forecast error range as the upper and lower bounds of control variables, which can be expressed as:

$$\begin{cases} \max \text{ or } \min V_i \\ \text{s.t. } V = PFC(\overline{P_G}, P_L, Q_L, CQ^*) \\ \quad \overline{P_G} = P_G(1+\xi) \\ \quad -\xi_{\max} \le \xi \le \xi_{\max} \end{cases} \tag{13}$$

where $PFC(\cdot)$ is the function for PF calculation; $\overline{P_G}$ is the random output of distributed energy; $CQ^*$ is the current optimal control strategy provided by the upper model; and $\xi$ and $\xi_{\max}$ are the deviation factor of distributed energy output and its maximum value, respectively.

The upper model is mainly to optimize the two extreme scenarios provided by the lower model, i.e., to find the optimal control strategy of reactive power equipment to achieve the optimal operations of the two extreme scenarios on the basis of meeting all the constraints, which can be expressed as:

$$\begin{cases} \min \left( \sum_{i=1}^{n} \| V_{Hi} - V_{i,tar} \|_2^2 + \sum_{i=1}^{n} \| V_{Li} - V_{i,tar} \|_2^2 \right) \\ \text{s.t. } V_H = PFC(P_{G,H}, P_L, Q_L, CQ) \\ \quad P_{G,H} = P_G(1+\xi_H) \\ \quad V_L = PFC(P_{G,L}, P_L, Q_L, CQ) \\ \quad P_{G,L} = P_G(1+\xi_L) \\ \quad V_{\min} \le V_H \le V_{\max} \\ \quad V_{\min} \le V_L \le V_{\max} \\ \quad CQ_{\min} \le CQ \le CQ_{\max} \end{cases} \tag{14}$$

where $V_H$ and $V_L$ are the node voltages obtained through $PFC$ using the current optimal control strategy in the two extreme scenarios provided by the lower model, respectively; $V_{\min}$ and $V_{\max}$ are the lower and upper limits of node voltages, respectively; $\xi_H$ and $\xi_L$ are the deviation factors corresponding to the two extreme scenarios, respectively; and $P_{G,H}$ and $P_{G,L}$ are the distributed energy output corresponding to the two extreme scenarios, respectively.

WSM-RVVC considers the two extreme scenarios formed by random variables in each iteration through the interaction between the upper and lower optimization models, so the final control strategy can completely eliminate the out-of-limit possibility caused by the uncertainty of distributed energy, achieve the optimal operation of the extreme scenarios, and has high robustness. However, WSM-RVVC still has the following disadvantages: ① to obtain the two extreme scenarios under the current control strategy, it has to complete the optimization of the maximum and minimum voltages of all nodes in each iteration, so the optimization of lower model is time-consuming; ② the objective function is not properly formulated. Although the actual output of distributed energy may deviate from the predicted value, the probability of extreme operation scenarios is usually very low. If only the two extreme scenarios are optimized, on the one hand, the optimization performance of the final actual operation scenario may be reduced. On the other hand, in each iteration of upper model, it has to complete two PF calculations to obtain the maximum and minimum voltage value, which takes more time.

### B. RVVC Using Convex DLIPF

In order to ensure the optimization accuracy of RVVC as well as the convenience and rapidity of its modeling and solution, this paper mainly modifies WSM-RVVC, and finally realizes the optimal control of the maximum probability operation scenario (MPOS) using convex DLIPF. Its core ideas are mainly summarized as follows.

1) ICNN is used again to directly form the convex mapping between the state parameters and the extreme voltage

value. That is, instead of WSM-RVVC which needs multiple optimizations of the lower model, the maximum and minimum node voltages caused by the uncertainty of random variables under the current control strategy can be obtained through only a single forward calculation of DLIPF model.

2) Since the operation value with the maximum probability of distributed energy is the median value of the forecasting range, this paper takes the scenario corresponding to the median value unit as RVVC object instead of WSM-RVVC directly taking the two extreme scenarios. To overcome the uncertainty brought by the random variables, the inequality constraints of the extreme voltage of each node, which are obtained from convex DLIPF, are directly added into the RVVC model.

The ICNN for the mapping of convex interval PF is named $ICNN_{EV}$. The parameters of $ICNN_{PF}$ and $ICNN_{EV}$ are set to be $\omega$ and $\theta$, respectively.

Based on the above core ideas, the main steps of convex DLIPF based RVVC method are as follows.

*Step 1*: training of sample generation for convex DLIPF. By randomly adjusting the node loads to be 0-1.2 times the normal level, the active power output of generators to be 0-1 times the rated power value, and the instructions of reactive equipment and deviation factor of distributed energy output to be the interval of upper and lower limits to form different scenarios, the input of training samples $[P_L, Q_L, P_G, C_Q, \xi]$ is formed. The maximum and minimum voltages of each node are obtained by WSM to form $[V_H, V_L]$ as the output of training samples. Then massive training samples can be obtained to conduct the supervised training of $ICNN_{EV}$. To minimize the generation time of training samples, $ICNN_{PF}$ continues to be adopted to replace the PF constraints, so the mathematical model of WSM can be expressed as:

$$\begin{cases} \max \text{ or } \min V_i \\ \text{s.t. } V = ICNN_{PF}(\overline{P_G}, P_L, Q_L, C_Q) \\ \quad \overline{P_G} = P_G(1+\xi) \\ \quad -\xi_{\max} \le \xi \le \xi_{\max} \end{cases} \tag{15}$$

*Step 2*: training of convex DLIPF. The massive training samples generated in the first step are input into ICNN for training. As the convex feature of ICNN, the network output (extreme node voltage) is also convex relative to the network input (state parameters and deviation factor of distributed energy output).

$$\begin{cases} J(\theta) = \sum_{i=1}^{m} (v_H(S'|\theta) - V_H(S'))^2 + (v_L(S'|\theta) - V_L(S'))^2 \\ S' = [P_L, Q_L, P_G, CQ, \xi] \\ \theta = \theta - \alpha \nabla J(\theta) \end{cases} \tag{16}$$

where $J$ is the training loss function; $m$ is the number of training samples; $v_H$, $v_L$ and $V_H$, $V_L$ are the predicted extreme voltages of $ICNN_{EV}$ and the true extreme voltages, respectively; $S'$ generated by WSM is the input variable set; and $\alpha$ is the learning rate.

*Step 3*: convex DLIPF based RVVC. As $ICNN_{EV}$ forms the direct mapping between state parameters and extreme voltage of each node, the lower model of WSM-RVVC can be completely eliminated, and the uncertainty caused by distributed energy can be transformed into the upper model by only generating the inequality constraints of the maximum and minimum voltages of each node through the forward calculation of $ICNN_{EV}$, Therefore, the finally established RVVC model can be expressed as:

$$\begin{cases} \min \sum_{i=1}^{n} \|V_i - V_{i,tar}\|_2^2 \\ \text{s.t. } V = ICNN_{PFC}(P_{G0}, P_L, Q_L, CQ) \\ \quad [V_H, V_L] = ICNN_{EV}(P_{G0}, P_L, Q_L, CQ, \xi) \\ \quad V_{\min} \le V_H \le V_{\max} \\ \quad V_{\min} \le V_L \le V_{\max} \\ \quad CQ_{\min} \le CQ \le CQ_{\max} \end{cases} \tag{17}$$

where $P_{G0}$ is the median value of the distributed energy forecasting range.

As can be obtained from the above modeling process, the convex DLIPF based RVVC uses $ICNN_{PFC}$ to replace the original PF constraints, and uses $ICNN_{EV}$ to replace the original lower optimization model, which effectively transforms the uncertainty of distributed energy. Due to the convex feature of ICNN, the objective function and constraints of the model are all convex, so it is much easier to solve the new type of RVVC. In addition, as long as the grid topology does not change, the established $ICNN_{PFC}$ and $ICNN_{EV}$ can be used repeatedly for different scenarios, and only the third step is required for each optimization, which truly realizes the convenience of RVVC modeling and solution.

## V. Numerical Tests

### A. Validation of Convex DLPF Based DVVC Method

The correctness and rapidity of convex DLPF based DVVC method are verified using the IEEE 118-bus system and Illinois 200-bus system of USA, whose detailed parameters are both obtained from MATPOWER toolbox of MATLAB. The control objects are the built-in generators. The target is to make the voltage of all nodes close to the value 1 p.u. and the voltage constraint is set to be [0.97, 1.03]p. u.. To evaluate the control effect of the proposed method, comparative experiments with different DVVC methods are carried out. The description of different DVVC methods used for comparison are listed in Table II, where interior point method (IPM) is the basic mathematical method for solving nonlinear optimization problems among them. The basic parameter settings, and numbers of variables and PF constraints of different DVVC methods are listed in Table III. Five hundred randomly generated scenarios are used to compare the control effects of different methods. The comparison indicators include the average voltage deviation (AVD), the average calculation time (ACT), and the success rate of DVVC.

Table IV and Table V show the comparisons of different DVVC methods for IEEE 118-bus and Illinois 200-bus systems in 500 different test scenarios, respectively.

TABLE II
DESCRIPTION OF DIFFERENT DVVC METHODS

| Method | Description |
|---|---|
| 1 | Convex DLPF + IPM (proposed method in this paper) |
| 2 | Pure IPM |
| 3 | SOC + IPM |

TABLE III
BASIC PARAMETER SETTING AND NUMBERS OF VARIABLES AND CONSTRAINTS

| Method | Parameter | Value |
|---|---|---|
| 1 | DL structure | [214, 500, 500, 118], [302, 600, 600, 200] |
| | Learning rate | 0.0003 |
| | Number of variables for two systems | 53, 48 |
| | Number of PF constraints for two systems | 1, 1 |
| 2 | Penalty factor | 0.1 |
| | Convergence precision | $10^{-6}$ |
| | Number of variables for two systems | 234, 398 |
| | Number of PF constraints for two systems | 181, 350 |
| 3 | Penalty factor | 0.1 |
| | Convergence precision | $10^{-6}$ |
| | Number of variables for two systems | 792, 1133 |
| | Number of PF constraints for two systems | 739, 1085 |

To exhibit the control effects of the three methods more clearly, Figs. 5(a) and 6(a) compare the AVD indicator of methods 1 and 2 corresponding to scenarios 1-100, while Figs. 5(b) and 6(b) show the comparison between methods 1 and 3. Since the AVD indicator is too large when DVVC fails using method 3, Figs. 5(c) and 6(c) provide a more detailed comparison of methods 1 and 3 for the scenarios where DVVC is successful using method 3.

TABLE IV
COMPARISON OF DIFFERENT DVVC METHODS FOR IEEE 118-BUS SYSTEM

| Method | Average AVD | | ACT (s) | Success rate (within voltage constraint) (%) |
|---|---|---|---|---|
| | With failure scenarios using method 3 | Without failure scenarios using method 3 | | |
| 1 | $2.18\times10^{-3}$ | $2.13\times10^{-3}$ | 0.087 | 100.0 |
| 2 | $2.36\times10^{-3}$ | $2.27\times10^{-3}$ | 4.380 | 100.0 |
| 3 | $10.84\times10^{-3}$ | $2.22\times10^{-3}$ | 256.410 | 83.8 |

TABLE V
COMPARISON OF DIFFERENT DVVC METHODS FOR ILLINOIS 200-BUS SYSTEM

| Method | Average AVD | | ACT (s) | Success rate (within voltage constraint) (%) |
|---|---|---|---|---|
| | With failure scenarios using method 3 | Without failure scenarios using method 3 | | |
| 1 | $2.66\times10^{-3}$ | $2.60\times10^{-3}$ | 0.16 | 100.0 |
| 2 | $2.80\times10^{-3}$ | $2.73\times10^{-3}$ | 6.93 | 100.0 |
| 3 | $11.55\times10^{-3}$ | $2.67\times10^{-3}$ | 380.31 | 77.4 |

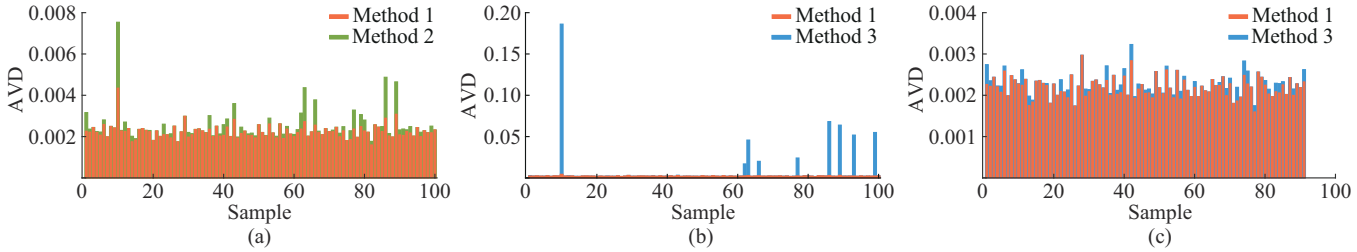


Fig. 5. AVD comparisons between different DVVC methods based on IEEE 118-bus system. (a) AVD comparison of methods 1 and 2. (b) AVD comparison of methods 1 and 3. (c) AVD comparison of methods 1 and 3 corresponding to scenarios where DVVC is successful using method 3.

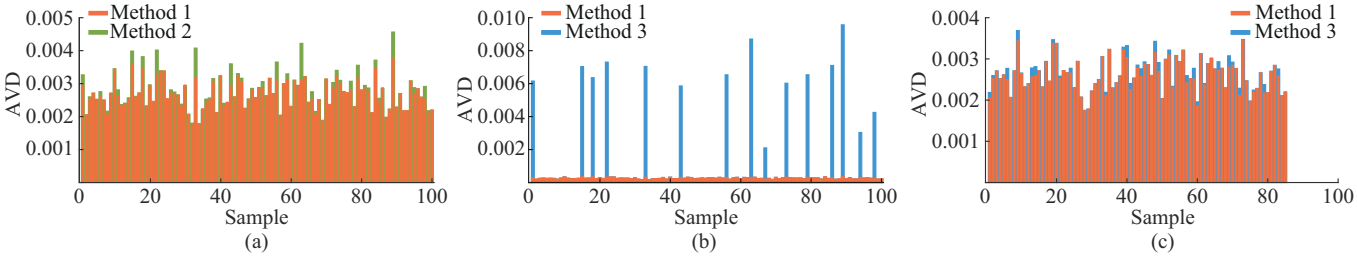


Fig. 6. AVD comparisons between different DVVC methods based on Illinois 200-bus system. (a) AVD comparison of methods 1 and 2. (b) AVD comparison of methods 1 and 3. (c) AVD comparison of methods 1 and 3 corresponding to scenarios where DVVC is successful using method 3.

The statistical numbers of optimization variables and PF constraints by the three DVVC methods shown in Table III are first analyzed. When solving directly by method 2, the variables to be solved include the voltage and phase angle of all nodes except the balance node, so the total variable numbers are $2(n-1)=234$ and 398 for the IEEE 118-bus and Illinois 200-bus systems, respectively; regarding PF constraints, the active power balance of all nodes except the balance node and the reactive balance of the load nodes need to be modeled, so the total constraint numbers are $2(n-1)-n_{PV}=$ 181 and 350, respectively. When using method 3, the variables to be solved increase the active power, the reactive power transmitted by the head node, and the current of each line, so the total variable numbers are $2(n-1)+3n_l=792$ and

1133, respectively. Regarding PF constraints, the voltage balance, head node power balance, and phase angle balance of each line need to be added, so the total constraint numbers are $2(n-1)-n_{PV}+3n_l=739$ and 1085, respectively.

Therefore, compared with the DVVC without convexity conversion, applying SOC to DVVC will greatly increase the numbers of variables and PF constraints. In contrast, when solving with the convex DLPF (method 1), since the end-to-end convex mapping between the state parameters and node voltage is established with the $ICNN_{PF}$, the number of PF constraints is only 1; regarding variables as the active and reactive power loads $P_L$ and $Q_L$, the active power outputs of generators $P_G$ are determined, and the variables to be solved are only the regulation states of reactive power equipment, which are the terminal voltage values of generators. As a result, the number of variables to be solved and the number of PF constraints to be handled can be significantly reduced by using convex DLPF.

Next, the statistical indicators of the three DPRO methods in Table IV and Table V are analyzed.

1) For the IEEE 118-bus system and Illinois 200-bus system, the success optimization rates of methods 1 and 2 are both 100%, while those of method 3 are only 83.8% and 77.4%, respectively. The reason is that convexity conversion by SOC makes the variables and PF constraints increase significantly, resulting in a significant increase in solution complexity and difficulty, and many control scenarios can not meet the voltage constraints. Therefore, Fig. 5(b) shows that the AVDs of several scenarios using method 3 form bumps that are much higher than those using method 1.

2) In terms of the average AVD indicator of 500 control scenarios, the average value of method 1 is the smallest whether ignoring the failure scenarios using method 3 or not. It proves that although the convex DLPF formed by convexity conversion of ICNN sacrifices the small error of node voltage, the control effect of DVVC will not be affected at all. The above conclusions can also be reflected in Figs. 5(a), 5(c), 6(a), 6(c) for all scenarios. The bumps obtained by the AVDs of several scenarios using method 1 are all lower than those using methods 2 and 3. In addition, the AVDs of several scenarios using method 2 (e.g., the 10th scenario of IEEE 118-bus system) are too far from that of method 1 in Fig. 5(a), which forms a much higher bump and proves the non-convexity of DVVC. The bumps formed by the AVDs of several scenarios using method 3 corresponding to the successful optimization scenarios are also higher than those using method 1, which proves that SOC can not guarantee the convergence to global optimum within the maximum iterations when the variables and PF constraints are too large.

3) In terms of ACT indicator, method 1 with only 0.087 s for IEEE 18-bus system and 0.16 s for Illinois 200-bus system is also the best, followed by method 2 with 4.38 s and 6.93 s, respectively. Method 3 with 256.41 s and 380.31 s is the worst, which shows that the computation speed of DVVC is not only related to the convexity, but also greatly affected by the number of optimization variables and PF constraints. With the convexity conversion by ICNN to form convex DLPF, the numbers of computation variables and PF constraints are greatly reduced, the computation speed of DVVC can be significantly improved. For IEEE 118-bus system, the computation speed of method 1 is 50.3 times that of method 2 and 2947.2 times that of method 3. For Illinois 200-bus system, the multiples are 43.3 and 2376.9, respectively.

### *B. Validation of Convex DLIPF Based RVVC Method*

The correctness and rapidity of convex DLIPF based RVVC method are verified using IEEE 30-bus system and Illinois 200-bus system, whose data are still from the MATPOWER toolbox of MATLAB. In order to verify that the proposed method can effectively eliminate the impact brought by the uncertainty of distributed energies, the two test systems are both assumed to be connected to distributed energies with different capacities, where the 26th and 30th nodes of IEEE 30-bus system are both connected to distributed energy resources with the capacity of 15 MVA, the 177th, 178th, 199th, 200th nodes of Illinois 200-bus system are connected to distributed energy resources with the capacity of 50 MVA, and the forecasting deviation range of active power output is set to be [–30%, 30%]. The control objects of the IEEE 30-bus system are generators and transformer taps, while those of the Illinois 200-bus system are the generators. The target is still to make the voltage of all nodes close to the value of 1 p.u.. Similar to DVVC, comparative experiments with different RVVC methods are carried out in this paper as well as comparisons with convex DLPF based DVVC method, which are all specified in Table VI. The control scenario of convex DLPF based RVVC is the MPOS which corresponds to the combination of the median values in the fluctuation range of all distributed energies. Similarly, 500 randomly generated scenarios are used to compare the control effects of different methods. The comparison indexes include average AVD and ACT.

TABLE VI
DESCRIPTION OF DIFFERENT RVVC METHODS

| Method | Description |
|---|---|
| 4 | Convex DLIPF based RVVC |
| 5 | WSM-RVVC |
| 6 | WSM + SOC based RVVC |

Table VII shows the comparison of different RVVC methods in terms of average AVD and ACT indicators of 500 test scenarios. To exhibit the control effects of the four methods more clearly, Figs. 7(a) and 9(a) compare the AVD indicators of methods 1 and 4 corresponding to 50 scenarios of IEEE 30-bus system and Illinois 200-bus system, respectively; Figs. 7(b) and 9(b) show the comparison between methods 4 and 5; and Figs. 7(c) and 9(c) show the comparison between methods 4 and 6. Figure 8 compares the operating range of node voltage corresponding to scenario 9 using methods 1 and 4 based on IEEE 30-bus system. Figure 10 is the corresponding comparison of scenario 11 based on Illinois 200-bus system.

TABLE VII
COMPARISON OF DIFFERENT RVVC METHODS

| Method | IEEE 30-bus system | | Illinois 200-bus system | |
|---|---|---|---|---|
| | Average AVD | ACT (s) | Average AVD | ACT (s) |
| 1 | $3.33\times10^{-3}$ | 0.058 | $2.68\times10^{-3}$ | 0.16 |
| 4 | $3.47\times10^{-3}$ | 0.147 | $2.77\times10^{-3}$ | 1.82 |
| 5 | $3.71\times10^{-3}$ | 12.170 | $2.87\times10^{-3}$ | 73.89 |
| 6 | $3.48\times10^{-3}$ | 50.250 | $2.80\times10^{-3}$ | 873.44 |

Due to the forecasting error of distributed energy, the set voltage constraint may not be met when using the reactive power equipment control strategy obtained by DVVC for the extreme scenarios. Therefore, the control strategy needs to be adjusted, but the impact is the worsening of MPOS control effect.

Therefore, it is easy to find the difference between the AVD using DVVC and RVVC for some scenarios in of Fig. 7(a) and 9(a). To illustrate the effectiveness of method 4 in more detail, for the scenario 9 of IEEE 30-bus system and the scenario 11 of Illinois 200-bus system with the largest difference, the voltage fluctuation ranges using methods 1 and 4 are drawn in Figs. 8 and 10, respectively.

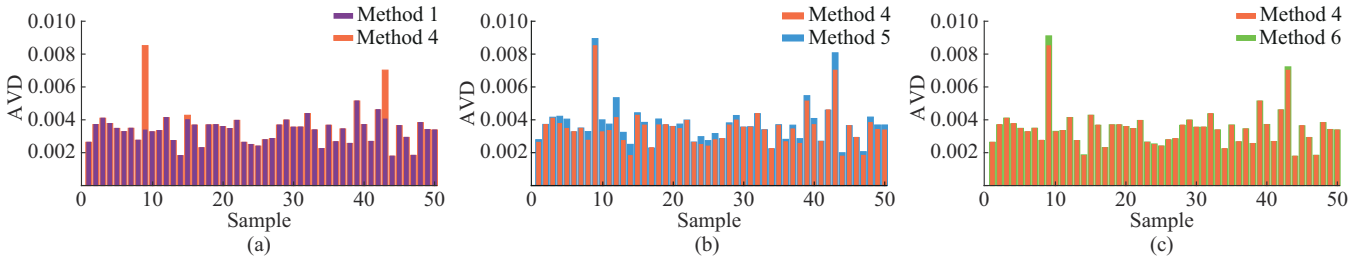


Fig. 7. AVD comparisons between different RVVC methods based on IEEE 30-bus system. (a) AVD comparison of methods 1 and 4. (b) AVD comparison of methods 4 and 5. (c) AVD comparison of methods 4 and 6.

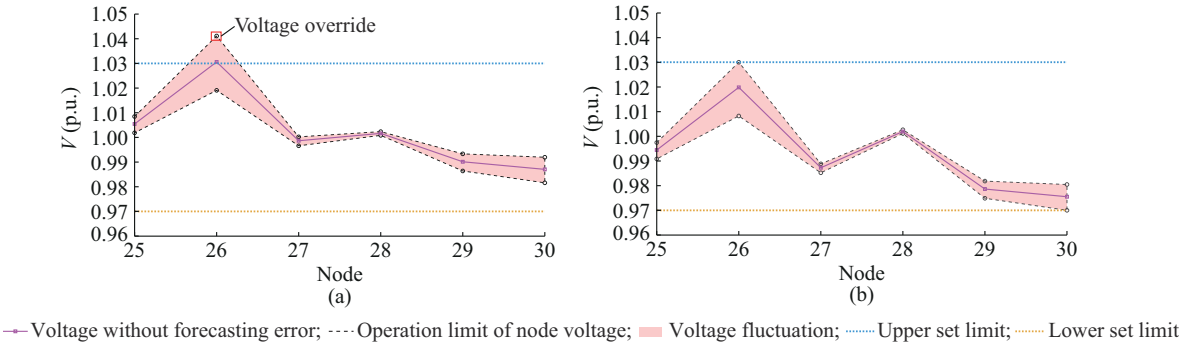


Fig. 8. Comparison of operating voltage range corresponding to scenario 9 using methods 1 and 4 based on IEEE 30-bus system. (a) Method 1. (b) Method 4.

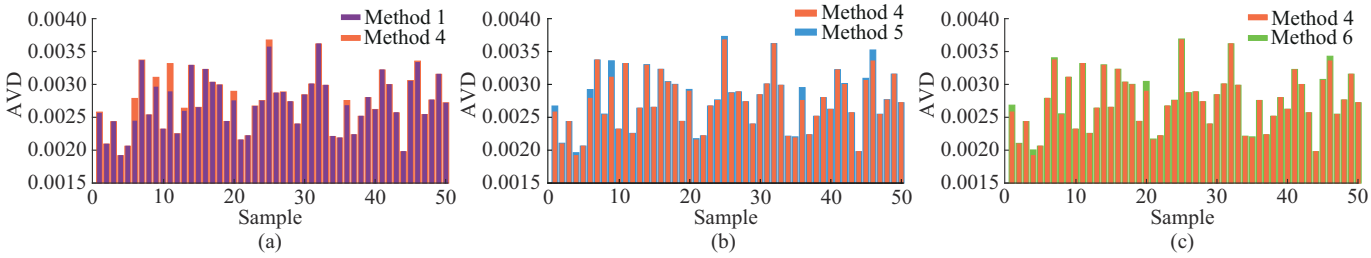


Fig. 9. AVD comparisons between different RVVC methods based on Illinois 200-bus system. (a) AVD comparison of methods 1 and 4. (b) AVD comparison of methods 4 and 5. (c) AVD comparison of methods 4 and 6.

Figures 8(a) and 10(a) show that when DVVC is adopted, although the node voltage of MPOS can be regulated to the set voltage constraint, due to the forecasting error of distributed energy, the maximum possible voltage of node 26 in IEEE 30-bus system can reach 1.041 p.u. and that of node 178 in Illinois 200-bus system can reach 1.035 p.u., which both exceed the set voltage constraint. Figures 8(b) and 10(b) show that when method 4 is adopted, the fluctuation range of each node can be adjusted within the set voltage constraint, proving that the impact of forecasting error on VVC can be effectively eliminated.

As observed from Figs. 7(b) and 9(b), since method 5 does not perform the convexity conversion, the robust optimization problem is non-convex, and the global optimum of the control strategy cannot be guaranteed, so the AVDs of MPOS obtained using method 5 are all inferior to those of method 4. As observed from Figs. 7(c) and 9(c), method 6 is the upgraded version of method 5 by adding the SOC based convexity conversion of PF constraints, and the robust optimization problem is convex. However, as mentioned above,

SOC significantly increases the numbers of optimization variables and PF constraints, resulting in a significant increase of the difficulty in solving. Therefore, for the scenarios that need to conduct robust optimization such as scenario 9 in IEEE 30-bus system and scenario 11 in Illinois 200-bus system, the AVDs of several scenarios using method 6 are still worse than those using method 4.

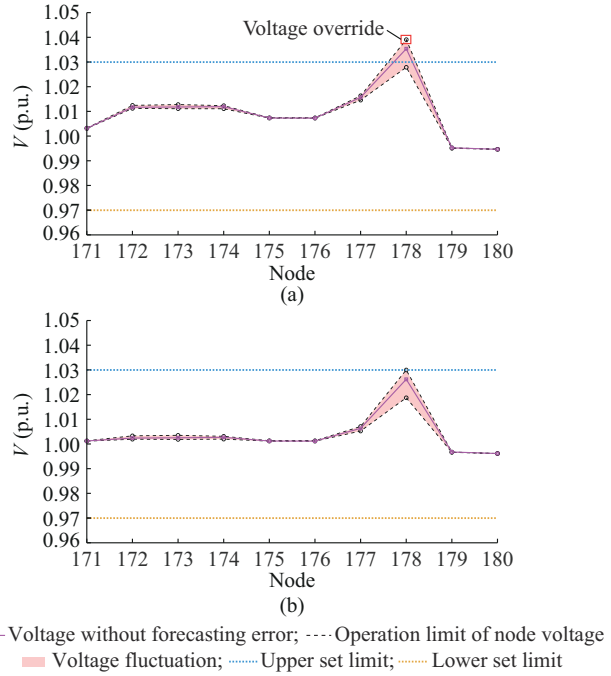


Fig. 10. Comparison of operating voltage range corresponding to scenario 11 using methods 1 and 4 based on Illinois 200-bus system. (a) Method 1. (b) Method 4.

In terms of computation speed, as observed in the Table VII, since method 4 eliminates the lower model of the traditional RVVC model which needs iterations to search the extreme scenarios, and uses the ICNN to establish the direct mapping between state parameters and extreme voltage, the calculation amount is greatly reduced. The ACTs of several scenarios using method 4 are only 0.147 s and 1.82 s for the IEEE 30-bus and Illinois 200-bus systems, respectively, and the computation speed is 82.9 times and 40.6 times that of method 5, 341.8 times and 479.9 times that of method 6, respectively.

## VI. Conclusion

A DVVC method based on convex DLPF is proposed in this paper. Different from SOC which makes the numbers of optimization variables and PF constraints greatly increase when applied to DVVC, this method only needs to use ICNN to establish a convex mapping (convex DLPF) between state parameters and node voltage to replace the traditional PF constraints, then the DVVC can be converted into a convex optimization problem. At the same time, the numbers of optimization variables and PF constraints are greatly reduced, which can greatly reduce the optimization difficulty. The experimental results based on IEEE 118-bus system verify the correctness and fast computation speed of the proposed method.

A convex DLIPF based RVVC method is proposed in this paper. Unlike the traditional RVVC which needs to conduct the search of two extreme scenarios to upgrade the current optimal control strategy of reactive power equipment, this method continues to use ICNN to establish a convex mapping between state parameters and node voltage interval, which can eliminate the iterative search of extreme scenarios of traditional RVVC. This method combines the two convexity maps of convex DLPF and convex DLIPF to realize the convexity conversion of RVVC, greatly simplifying the modeling and optimization difficulty of robust optimization. The experimental results based on IEEE 30-bus system verify the superiority of the proposed method.

Compared with traditional DVVC and RVVC, this paper introduces ICNN to achieve the transformation of PF constraints and robust optimization constraints brought by distributed energy access, eliminating many complex modeling operations and calculation steps of existing methods, greatly simplifying the modeling process, and improving computation speed. Unlike other methods (such as reinforcement learning [32] and generative adversarial network (GAN) [33]) dedicated to establishing the end-to-end mapping between system states and control method without no convexity conversion, the convex feature of ICNN introduced in this paper also ensures the optimality of the control method. The limitation of the proposed method is that the convex mappings formed by ICNN need to be generated in advance, which takes some time. But these mappings only need to be trained offline once and can be repeatedly used when applied to online calculation. In the future, we will conduct further research on how the proposed method in this paper can be applied to unbalanced distribution networks and other optimization problems with PF constraints and robust constraints such as power dispatching problem.

## References

[1] A. Bedawy, N. Yorino, K. Mahmoud *et al.*, "Optimal voltage control strategy for voltage regulators in active unbalanced distribution systems using multi-agents," *IEEE Transactions on Power Systems*, vol. 35, no. 2, pp. 1023-1035, Mar. 2020.

[2] M. H. J. Bollen, R. Das, S. Djokic, *et al.*, "Power quality concerns in implementing smart distribution-grid applications," *IEEE Transactions on Smart Grid*, vol. 8, no. 1, pp. 391-399, Jan. 2017.

[3] F. U. Nazir, B. C. Pal, and R. A. Jabr, "Affinely adjustable robust volt/var control without centralized computations," *IEEE Transactions on Power Systems*, vol. 38, no. 1, pp. 656-667, Jan. 2023.

[4] F. U. Nazir, B. C. Pal, and R. A. Jabr, "Distributed solution of stochastic volt/var control in radial networks," *IEEE Transactions on Smart Grid*, vol. 11, no. 6, pp. 5314-5324, Nov. 2020.

[5] S. E. Kayacık and B. Kocuk, "An MISOCP-based solution approach to the reactive optimal power flow problem," *IEEE Transactions on Power Systems*, vol. 36, no. 1, pp. 529-532, Jan. 2021.

[6] M. Chowdhury and S. Kamalasadan, "A new second-order cone programming model for voltage control of power distribution system with inverter-based distributed generation," *IEEE Transactions on Industry Applications*, vol. 57, no. 6, pp. 6559-6567, Nov. 2021.

[7] D. Hu, Z. Ye, Y. Gao *et al.*, "Multi-agent deep reinforcement learning for voltage control with coordinated active and reactive power optimization," *IEEE Transactions on Smart Grid*, vol. 13, no. 6, pp. 4873-4886, Nov. 2022.

[8] X. Sun, J. Qiu, Y. Tao *et al.*, "Coordinated real-time voltage control in active distribution networks: an incentive-based fairness approach," *IEEE Transactions on Smart Grid*, vol. 13, no. 4, pp. 2650-2663, Jul. 2022.

[9] Y. Bai, H. Zhong, Q. Xia *et al.*, "A two-level approach to AC optimal transmission switching with an accelerating technique," *IEEE Transactions on Power Systems*, vol. 32, no. 2, pp. 1616-1625, Mar. 2017.
[10] A. F. Soofi, S. D. Manshadi, G. Liu *et al.*, "A SOCP relaxation for cycle constraints in the optimal power flow problem," *IEEE Transactions on Smart Grid*, vol. 12, no. 2, pp. 1663-1673, Mar. 2021.
[11] X. Hu, H. Hu, S. Verma *et al.*, "Physics-guided deep neural networks for power flow analysis," *IEEE Transactions on Power Systems*, vol. 36, no. 3, pp. 2082-2092, May 2021.
[12] Y. Yang, Z. Yang, J. Yu *et al.*, "Fast calculation of probabilistic power flow: a model-based deep learning approach," *IEEE Transactions on Smart Grid*, vol. 11, no. 3, pp. 2235-2244, May 2020.
[13] S. Zhang and J. Yu, "Bayesian deep learning for dynamic power system state prediction considering renewable energy uncertainty," *Journal of Modern Power Systems and Clean Energy*, vol. 10, no. 4, pp. 913-922, Jul. 2022.
[14] Q. Chai, C. Zhang, Y. Xu *et al.*, "PV inverter reliability-constrained volt/var control of distribution networks," *IEEE Transactions on Sustainable Energy*, vol. 12, no. 3, pp. 1788-1800, Jul. 2021.
[15] F. U. Nazir, B. C. Pal, and R. A. Jabr, "A two-stage chance constrained volt/var control scheme for active distribution networks with nodal power uncertainties," *IEEE Transactions on Power Systems*, vol. 34, no. 1, pp. 314-325, Jan. 2019.
[16] T. Ding, Q. Yang, Y. Yang *et al.*, "A data-driven stochastic reactive power optimization considering uncertainties in active distribution networks and decomposition method," *IEEE Transactions on Smart Grid*, vol. 9, no. 5, pp. 4994-5004, Sept. 2018.
[17] M. Bazrafshan and N. Gatsis, "Decentralized stochastic optimal power flow in radial networks with distributed generation," *IEEE Transactions on Smart Grid*, vol. 8, no. 2, pp. 787-801, Mar. 2017.
[18] C. Zhang, H. Chen, Z. Liang *et al.*, "Reactive power optimization under interval uncertainty by the linear approximation method and its modified method," *IEEE Transactions on Smart Grid*, vol. 9, no. 5, pp. 4587-4600, Sept. 2018.
[19] S. Abadi, A. Attarha, P. Scott *et al.*, "Affinely adjustable robust volt/var control for distribution systems with high PV penetration," *IEEE Transactions on Power Systems*, vol. 36, no. 4, pp. 3238-3247, Jul. 2021.
[20] K. Christakou, M. Paolone, and A. Abur, "Voltage control in active distribution networks under uncertainty in the system model: a robust optimization approach," *IEEE Transactions on Smart Grid*, vol. 9, no. 6, pp. 5631-5642, Nov. 2018.
[21] T. Ding, S. Liu, W. Yuan *et al.*, "A two-stage robust reactive power optimization considering uncertain wind power integration in active distribution networks," *IEEE Transactions on Sustainable Energy*, vol. 7, no. 1, pp. 301-311, Jan. 2016.
[22] C. Zhang, Y. Xu, Z. Dong *et al.*, "Three-stage robust inverter-based voltage/var control for distribution networks with high-level PV," *IEEE Transactions on Smart Grid*, vol. 10, no. 1, pp. 782-793, Jan. 2019.
[23] H. Gao, J. Liu, and L. Wang, "Robust coordinated optimization of active and reactive power in active distribution systems," *IEEE Transactions on Smart Grid*, vol. 9, no. 5, pp. 4436-4447, Sept. 2018.
[24] J. Liu, Y. Chen, C. Duan *et al.*, "Distributionally robust optimal reactive power dispatch with Wasserstein distance in active distribution network," *Journal of Modern Power Systems and Clean Energy*, vol. 8, no. 3, pp. 426-436, May 2020.
[25] C. Zhang, H. Chen, and H. Ngan, "Reactive power optimization considering wind farms based on an optimal scenario method," *IET Generation, Transmission & Distribution*, vol. 10, no. 15, pp. 3736-3744, Nov. 2016.
[26] Q. Hui, Y. Teng, H. Zuo *et al.*, "Reactive power multi-objective optimization for multi-terminal AC/DC interconnected power systems under wind power fluctuation," *CSEE Journal of Power and Energy Systems*, vol. 6, no. 3, pp. 630-637, Sept. 2020.
[27] R. A. Jabr, "Adjustable robust OPF with renewable energy sources," *IEEE Transactions on Power Systems*, vol. 28, no. 4, pp. 4742-4751, Nov. 2013.
[28] B. Amos, L. Xu, and J. Z. Kolter, "Input convex neural networks," in *Proceedings of International Conference on Machine Learning*, Singapore, Feb. 2017, pp. 146-155.
[29] Y. Chen, Y. Shi, and B. Zhang, "Optimal control via neural networks: a convex approach," in *Proceedings of International Conference on Learning Representations*, New Orleans, USA, May 2019, pp. 1-21.
[30] K. He, X. Zhang, S. Ren *et al.*, "Deep residual learning for image recognition," in *Proceedings of IEEE Conference on Computer Vision and Pattern Recognition*, Las Vegas, USA, Jun. 2016, pp. 770-778.
[31] S. Boyd and L. Vandenberghe, *Convex Optimization*. Cambridge: Cambridge University Press, 2004.
[32] J. Duan, D. Shi, R. Diao *et al*., "Deep-reinforcement-learning-based autonomous voltage control for power grid operations," *IEEE Transactions on Power Systems*, vol. 35, no. 1, pp. 814-817, Jan. 2020.
[33] J. Wang and P. Srikantha, "Fast optimal power flow with guarantees via an unsupervised generative model," *IEEE Transactions on Power Systems*, vol. 38, no. 5, pp. 4593-4604, Sept. 2023.

**Qing Ma** received the B.S. and M.S. degrees in electrical engineering from Wuhan University, Wuhan, China, in 2012 and 2015, respectively. He worked at State Grid Jiangxi Electric Power Company, Nanchang, China, for four years. He is currently pursuing the Ph.D. degree in electrical engineering at Wuhan University. His research interests include volt-var control of power system and application of artificial intelligence in power system.

**Changhong Deng** received the Ph.D. degree from the School of Electrical Engineering, Wuhan University, Wuhan, China, in 2005. She is currently a Professor at Wuhan University. Her research interests include power system security and stability analysis, and grid control with renewable energy integration.